Non-Hermitian swallowtail catastrophe revealing transitions across diverse topological singularities

Jing Hu[1,#], Ruo-Yang Zhang[1,#], Yixiao Wang[1], Xiaoping Ouyang[4], Yifei Zhu[3]*, Hongwei Jia[1,2]*, C. T. Chan[1,2]*

[1]Department of Physics, the Hong Kong University of Science and Technology, Clear Water Bay, Kowloon, Hong Kong, China

[2]Institute for Advanced Study, the Hong Kong University of Science and Technology, Clear Water Bay, Kowloon, Hong Kong, China

[3]Department of Mathematics, Southern University of Science and Technology, Shenzhen, Guangdong, China

[4]School of Materials Science and Engineering, Xiangtan University, Xiangtan, Hunan, China

[#]These authors contribute equally to this work

Exceptional points are a unique feature in non-Hermitian systems, where eigenvalues and their corresponding eigenstates of a Hamiltonian coalesce[1-12]. A lot of intriguing physical phenomena arise from the topology of exceptional points, such as "bulk Fermi-arcs"[2,3] and braiding of eigenvalues[10]. Here we report that a more exotic and structurally richer degeneracy morphology, known as the swallowtail catastrophe in singularity theory[13], can naturally exist in non-Hermitian systems with both parity-time and pseudo-Hermitian symmetries. The swallowtail exhibits the coexistence and intriguing interactions of degeneracy lines of three different types, including an isolated nodal line, a pair of exceptional lines of order three and a non-defective intersection line, with the

latter two types lying entirely on the exceptional surface. Surprisingly, these *a priori* independent types of singularities are stably connected at a single point, i.e. the vertex of the swallowtail, revealing mutual transitions among them. Moreover, we realized such systems in a non-reciprocal circuit and experimentally observed the degeneracy features of the swallowtail. Based on the frame rotation and deformation of eigenstates, we further demonstrated in theory and experiments that the various transitions are topologically protected. Our findings constitute the first demonstration of a swallowtail structure in band dispersions, *en route* establishing a whole new family of non-Hermitian topological phases of matter. The transitions across diverse singularities pave new avenues for the development of sensing and absorbing devices[14,15].

Main: In recent years, non-Hermitian systems have attracted a great deal of interest. A main goal is to address the ubiquitous open quantum systems that carry energy exchanges with the surrounding environment via the imaginary part of their eigen-energies[1-12]. Degenerate singularities in band structures are similar to topological defects in real space. Well-known singularities in Hermitian systems are Weyl/Dirac points and nodal lines[16-21], and their associated phenomena, such as topological edge modes[16,21] and chiral Landau levels[19] have been fully explored. In non-Hermitian systems, the complex nature of eigenvalues results in more exotic singularities such as exceptional points, at which two or more eigenstates coalesce. Exceptional points can carry fractional topological invariants, which not only enriches the topology classes in band theories[2,3,5,6], but also induces more intriguing physical consequences, such as "bulk-Fermi arcs"[2,3] and braiding of eigenvalues[10]. In addition, the skin effect, which is associated with the point gaps in non-Hermitian bands, is also a unique feature of non-Hermitian systems[22-24].

In non-Hermitian systems with parity-time (*PT*) symmetry or chiral symmetry, exceptional surfaces (ES) can stably exist as singular hypersurfaces in three-dimensional (3D)

parameter space, acting as boundaries between exact and broken phases[14,25,26]. Remarkably, as subspaces of parameter space, these exceptional surfaces afford numerous new singularities, such as high-order exceptional points (or lines) appearing as cusps[6,9], and non-defective degeneracies that are intersections of exceptional surfaces[8,11,12]. The co-existence of diverse singularities brings the possibility that they can be associated with each other. However, previous works commonly focused on a single type. The mutual transitions across different types, as well as the underlying topological structure, remain largely unexplored.

It was previously reported that in Hermitian systems with *PT* symmetry, the eigenstates form the basis of a Euclidean space and rotate in a non-Abelian way, giving rise to isolated nodal lines described by quaternion topological charges[20], which has been experimentally observed in a recent work[21]. Here, we transform the Euclidean geometry to a Riemannian geometry with non-Hermitian settings, where emerges a more exotic and structurally much richer degeneracy morphology, known as the swallowtail catastrophe in singularity theory[13]. The swallowtail is one of the elementary catastrophes in Arnold's ADE classification[13,27,28] and has been widely applied in many branches of physics and engineering, ranging from mechanics[29] to caustics of light[30]. However, it was never studied in eigenvalue dispersions before. Here we discover for the first time that the swallowtail catastrophe, which naturally exists in non-Hermitian systems with *PT* symmetry together with a pseudo-Hermitian symmetry, encompasses degeneracy lines of three different types. In addition to an isolated nodal line (NL) similar to the Hermitian case, it also includes a pair of exceptional lines of order three (EL3) and a non-defective intersection line (NIL) which lie entirely on the exceptional surface. Surprisingly, these *a priori* independent types of singular lines are stably connected at a single point of the swallowtail, revealing interesting mutual transitions among them. By realizing such systems in a non-reciprocal circuit, we experimentally observed the degeneracy features of the swallowtail. Furthermore, the mutual transitions across different

types of singularities complying with the topological constraints associated with them are demonstrated both theoretically and experimentally.

The three-state non-Hermitian Hamiltonian we considered takes the following form

$$H=\begin{pmatrix} -f_1-f_2+1 & -f_1 & -f_2 \\ f_1 & f_1+f_3 & -f_3 \\ f_2 & -f_3 & f_2+f_3 \end{pmatrix} \tag{1}$$

where $f_1 f_2 f_3$ are three real numbers specifying three degrees of freedom and defining a 3D parameter space. With the form in Eq. (1), the Hamiltonian preserves two symmetries[1]

$$\eta H \eta^{-1}=H^{\dagger}, \quad [H, PT]=0 \tag{2}$$

Here the first relation shows that H is η-pseudo-Hermitian with $\eta=\mathrm{diag}(-1,1,1)$. The Hamiltonian is required to be real, which is equivalent to the PT symmetry if we set the parameter space as the momentum space. We note that two off-diagonal elements are anti-symmetric ($H_{12}=-H_{21}$, $H_{13}=-H_{31}$), representing non-reciprocal hoppings between nodes. On the contrary, the other off-diagonal element is symmetric ($H_{23}=H_{32}$), and represents a reciprocal hopping. The degenerate surfaces and lines in the eigenvalue structure form a swallowtail as shown in Fig. 1a (see ADE description in Section 2 of supplementary information). The ES (red surfaces) and EL3s (black lines) results from the PT symmetry[9] of the system. The pair of EL3s merge at the meeting point (MP, red star), which simultaneously emits the non-defective degenerate NL and NIL (blue lines) in different directions. The NL is isolated from ESs, but the NIL is a complete intersection of ESs[8,11,12]. Owing to the two symmetries of the system in Eq. (2), the NL and NIL cannot be extended into a tube or cone in parameter space. Thus their stability is symmetry-protected (see Section 3-5 in supplementary information for demonstration). Therefore, the swallowtail is an assembly of diverse singularities (ES, EL3, NIL, NL and MP), and the two symmetries protect its stability.

The EL3 are lines at which two ESs meet, forming cusps. In catastrophe theory, a cusp is formed due to the projection of a folded curve (or surface) onto a lower dimensional space. Such a folding process can also be observed in non-Hermitian eigenvalue structures. On the cut plane f_3=0.3 (Fig. 1b), the red line (ES) is folded in the Reω-f_1-f_2 space. Thus, swapping of eigenvalues will occur if an observation point moving on the exceptional surface (as system parameter changes) passes through an EL3 (Section 6 of supplementary information). The NIL is also a coalescence of two ESs, and the nearby dispersion forms a double cone (inset of Fig. 1b), distinct from the EL3s. The pair of EL3s and the NIL are connected by ESs, forming a closed loop. Tuning the parameters (e.g. f_3=0.1214) makes the loop shrinkable, which provides a geometrical understanding that EL3s and NIL can merge at the MP (Fig. 1c). The MP can also be understood as a collision of a ray (NL) onto a surface (ES). Before the collision, the NL is totally isolated from the ES (see Fig. 1d for f_3=0.01), and the collision makes the ES non-differentiable at MP. Since both the NL and ES share the 2nd band (blue surface in Fig. 1d), the tuning of system parameters can make them collide.

To observe the exotic swallowtail and investigate the topological origin of the evolution of degeneracy features in parameter space, a non-reciprocal electric circuit system emulating the interaction of three nodes (labeled by **A**, **B** and **C**) was employed to realize the three-state non-Hermitian Hamiltonian (Fig. 2). Benefiting from a wide range of active circuit elements such as operational amplifiers, a circuit system is more flexible than other platforms if we need to accurately control gain, loss, as well as implementing non-reciprocal hopping. The behavior of a circuit system can be described by the Laplacian $\mathbf{I} = \boldsymbol{J}\mathbf{V}$ ($\boldsymbol{J}$: Admittance matrix, **I**: vector of input currents, and **V**: vector of node voltages)[23]. The admittance matrix $\boldsymbol{J}$ plays the role of the Hamiltonian matrix and its eigenvalues (admittance bands j) represent the energy bands. Thus, the synthetic dimensions of the parameter space, f_1, f_2 and f_3, can be mapped to the tight-binding hopping parameters between each pair of the circuit nodes (Fig. 2a). The circuit

element structure is shown in Fig. 2b. The non-reciprocal hoppings $\pm f_1$ (or $\pm f_2$) between the nodes **A** and **B** (or **A** and **C**) are implemented and controlled precisely by an impedance converter through current inversion (INIC) tandem with elements of capacitance C_1 (or C_2) supplementary information (Fig. 2c). Pure elements of capacitance C_3 realize the reciprocal hopping f_3 between **B** and **C**. One can properly select the values of C_1, C_2 and C_3 in the experiments to implement the required parameters of f_1, f_2 and f_3, respectively. A photo of the printed circuit board (PCB) for the experiments is presented in Fig. 2d. By measuring the voltage response of each node to a local a.c. current input, the admittance eigenvalues and eigenstates can be acquired. More details on experiments are shown in Section 1 of supplementary information.

Figure 3a1 shows the ESs, EL3s and NIL obtained from the experimental measurements (point marks), falling on the intersecting curve of the swallowtail on the plane f_3=0.3. These singularities are extracted from the measured admittance eigenvalues (circle marks, Fig. 3a2) as a function of f_1 along different lines ($f_2=f_1+s$) on the plane f_3=0.3. ESs can be clearly recognized from the quadratic coalescence of two eigenvalues in the experimental results, and two ESs (one formed by the 1nd and 2rd bands, and the other by 2nd and 3rd bands) form cusps at EL3s, which is observed experimentally as the merging of all the three eigenvalues. The NIL can be viewed as the complete intersection of two nonparallel ESs as indicated by Fig. 3a1 (both formed by the 2nd and 3rd bands), and is a linear degeneracy in the eigenvalue dispersion (Fig. 3a2). As f_3 descends to 0.1214, the exact phase domain enclosed by the ESs will shrink to the MP (Fig. 3b1), being the coincident point of a linear degeneracy and a quadratic coalescence of eigenvalues (Fig. 3b2). Continuing lowering f_3 to 0.01, the ESs and the MP are decoupled into an isolated singularity (NL) and a smooth ES (Fig. 3c). Likewise, the measured admittance eigenvalues in Fig. 3c2 indicates that the NL is a linear degeneracy of the 1nd and 2rd bands, and the ES is formed by the 2nd and 3rd bands. Apparently, the MP plays a pivotal

role in linking up all these degeneracy lines. To directly observe how the degeneracy lines and surfaces are connected at the MP, we further measured the eigenvalues on the plane $f_1=f_2$ (yellow plane, Fig. 1a) that contains all of them. Figure 3d1 illustrates that the NIL and NL are smoothly connected by the MP, which also serves as a tangent point to an ES and thus separates the ES into the upper and lower parts that are formed by the degeneracies of different bands (Fig. 3d2).

We now consider the topological aspects of the transition among different singular lines. The swallowtail implicitly exhibits several transition processes among symmetry-protected degeneracies supplementary information, and here we focus on the most interesting transition, i.e. from the pair of EL3s to the NIL and NL. Our target is to demonstrate that the pair of EL3s is topologically equivalent to the NIL and NL. We therefore consider the green loop l_α (on plane $f_3=0.3$, Fig. 4a1) encircling the pair of EL3s, and the yellow loop l_β (on plane $f_1+f_2=0.3$, Fig. 4b1) that encloses the NIL and NL together. Both loops inevitably cut through the ESs, as the EL3s and NIL are hypersurface singularities. Such an approach employs notions of intersection homotopy[31], which is different from the conventional homotopy description with encircling loops on which all the Hamiltonians are gapped (see details in Section 4 of supplementary information). The two loops have the same staring point (SP, purple dots) so that direct comparison can be performed. The equivalence between l_α and l_β is manifested by observing the eigen-frame rotation and deformation processes. The frame rotation concept has been used to label different NLs in multiband Hermitian systems with PT symmetry[20,21], in which the eigenstates form the orthogonal bases of a Euclidean space. Here in our system, the Euclidean geometry is no longer applicable. Conversely the symmetries (Eq. 2) reveals that the right eigenstates satisfy the following orthogonal relation

$$\varphi_m^T \eta \varphi_n \begin{cases} = 0 & m \neq n \\ \neq 0 & m = n \end{cases} \tag{3}$$

where the superscript *T* denotes transpose. Since η has the same form as the Minkowski metric, and the Hamiltonian is *PT*-symmetric (Eq. 1), the right eigenstates φ_m are analogous to the frame fields in general relativity (i.e. Riemannian geometry)[32]. Hence, eigenstates will experience Lorentz-like transformations as parameters vary (see details in Section 4 of supplementary information), which induces both frame rotation and frame deformations.

The trajectories of eigenvalues along loops l_α and l_β are shown in Fig. 4a2 and 4b2 respectively, and the corresponding evolution of eigenstates are provided by the trajectories of the ball markers in Figs. 4a3-4b3, where the three axes denote the three components of the eigenstates. The experimental and theoretical results are shown in the upper and lower panels, respectively. The three eigenstates φ_1, φ_2 and φ_3 are marked with red, blue and black balls, respectively, and the increase of the markers' size denotes the evolution process as the parameters vary along the loop. The eigenstates (according to normalization of Eq. S26 in supplementary information) need a rescaling in order to place the tip of the vector on a unit sphere. As indicated, the initial and final imaginary parts of eigenstates are all zero, suggesting that the evolution of the imaginary parts is simply an intermediate process. Thus the topology is dominantly characterized by the evolution of the real parts of eigenstates, which determines the rotation direction and rotation angle of the eigen-frame. It is revealed that along both loops, the accumulated rotation angle of φ_2 (blue) is zero, and both φ_1 and φ_3 experience π rotations, i.e. they evolve from the initial states to their antipodal points (as indicated by the green radial axis), resulting from the *PT* symmetry of the system. The results show that both loops can be viewed as topologically non-trivial as the rotation angles of the eigen-frame are quantized. From the starting point, we observe that φ_2 and φ_3 are rotating in opposite directions, which is a typical frame deformation process. In contrast, the rotating eigenstates must rotate in the same sense in a pure eigenframe rotation, which is typical for *PT*-symmetric

Hermitian systems[20,21]. The intermediate processes along l_α and l_β are slightly different from each other simply because they are along different trajectories. Therefore, the rotations of φ_1 and φ_3 along both loops are the same, which demonstrates that l_α is equivalent to l_β, and explains why the pair of EL3s can transit to the NIL and NL via the MP (Fig. 4c). Note that the SP of l_α and l_β do not need to be the same point so that the yellow and green loops in Fig. 4c do not need to touch in order for them to the have the same frame rotation/deformation (see the criteria discussed in Section 7 of supplementary information). The continuous deformation from l_α to l_β is shown in the movie. The analysis indicates that the transition is topologically protected. Our method based on Lorentz-like transformation of eigenstates also shows that the emergence of the swallowtail is allowed by the symmetries (Eq. 2).

To summarize, we showed that the swallowtail, which plays an important role in catastrophe theory, appears naturally in non-Hermitian systems when we consider the evolution of eigenvalues in parameter space. In a three-state *PT*-symmetric non-Hermitian system with an additional pseudo-Hermitian symmetry, we found degeneracies of eigenvalues in the form of EL3s, NIL and NL, and these seemingly unrelated types of singularities are stably connected at an MP, forming a swallowtail and can convert to each other as system parameter changes. From the experimental observations and theoretical analysis, we understand that the transition occurs because these singular lines are topologically associated with each other. Since the symmetries of the considered Hamiltonian play an important role in the emergence of the swallowtail, it is worthwhile to explore the generic topological classification of these symmetry-protected catastrophe singularities in the future. In addition, realizing such Hamiltonians in lattice systems could be valuable platforms for investigating the bulk-edge correspondence in non-Hermitian systems. The transitions across diverse singularities also pave new avenues for the development of sensing and absorbing devices[14,15].

References:

1. Kawabata, K., Shiozaki, K., Ueda, M. & Sato, M. Symmetry and topology in non-Hermitian physics. *Phys. Rev. X* **9**, 041015 (2019).

2. Zhou, H., et al. Observation of bulk Fermi arc and polarization half charge from paired exceptional points. *Science* **359**, 1009-1012 (2018).

3. Kawabata, K., Bessho, T. & Sato, M. Classification of exceptional points and non-Hermitian topological semimetals. *Phys. Rev. Lett.* **123**, 066405 (2019).

4. Miri, M. A., Alu, A., Exceptional points in optics and photonics. *Science* **363**, eaar7709 (2019).

5. Bergholtz, E. J., Budich, J. C. & Kunst, F. K. Exceptional topology of non-Hermitian systems. *Rev. Mod. Phys.* **93**, 015005 (2021).

6. Tang, W., et al. Exceptional nexus with a hybrid topological invariant. *Science* **370**, 1077-1080 (2020).

7. Shen, H., Zhen, B. & Fu, L. Topological band theory for non-Hermitian Hamiltonians. *Phys. Rev. Lett.* **120**, 146402 (2018).

8. Cui, X., et al. Symmetry-protected topological exceptional chains in non-Hermitian crystals. arXiv preprint arXiv:2204.08052, 2022.

9. Delplace, P., Yoshida, T. & Hatsugai, Y. Symmetry-protected multifold exceptional points and their topological characterization. *Phys. Rev. Lett.* **127**, 186602 (2021).

10. Wang, K., Dutt, A., Wojcik, C. C. & Fan, S. Topological complex-energy braiding of non-Hermitian bands. *Nature* **598**, 59-64 (2021).

11. Xiao, Y. X., et al. Exceptional points make an astroid in non-Hermitian Lieb lattice: Evolution and topological protection. *Phys. Rev. B* **102**, 245144 (2020).

12. Sayyad, S., Stalhammar, M., Rodland, L. & Kunst, F. K. Symmetry-protected exceptional and nodal points in non-Hermitian systems. arXiv preprint arXiv:2204.13945, 2022.

13. Arnol'd, V. I. *Catastrophe theory* (Springer Science & Business Media, 2003).

14. Zhong, Q., et al. Sensing with exceptional surfaces in order to combine sensitivity with robustness. *Phys. Rev. Lett.* **122**, 153902 (2019).

15. Soleymani, S., et al. Chiral and degenerate perfect absorption on exceptional surfaces. *Nat. Commun.* **13**, 1-8 (2022).

16. Wan, X., Turner, A. M., Vishwanath, A. & Savrasov S. Y. Topological semimetal and Fermi-arc surface states in the electronic structure of pyrochlore iridates. *Phys. Rev. B* **83**, 205101 (2011).

17. Young, S. M. & Kane, C. L. Dirac semimetals in two dimensions. *Phys. Rev. Lett.* **115**, 126803 (2015).

18. Chiu, C. K., Teo, J. C. Y., Schnyder, A. P. & Ryu, S. Classification of topological quantum matter with symmetries. *Rev. Mod. Phys.* **88**, 035005 (2016).

19. Jia, H., et al. Observation of chiral zero mode in inhomogeneous three-dimensional Weyl metamaterials. *Science* **363**, 148-151 (2019).

20. Wu, Q. S., Soluyanov, A. A. & Bzdušek, T. Non-Abelian band topology in noninteracting metals. *Science* **365**, 1273-1277 (2019).

21. Guo, Q., et al. Experimental observation of non-Abelian topological charges and edge states. *Nature* **594**, 195-200 (2021).

22. Okuma, N., Kawabata, K., Shiozaki, K. & Sato, M. Topological origin of non-Hermitian skin effects. *Phys. Rev. Lett.* **124**, 086801 (2020).

23. Helbig, T., et al. Generalized bulk–boundary correspondence in non-Hermitian topolectrical circuits. *Nat. Phys.* **16**, 747-750 (2020).

24. Yao, S. & Wang, Z. Edge states and topological invariants of non-Hermitian systems. *Phys. Rev. Lett.* **121**, 086803 (2018).

25. Zhang, X., et al. Experimental observation of an exceptional surface in synthetic dimensions with magnon polaritons. *Phys. Rev. Lett.* **123**, 237202 (2019).

26. Okugawa, R. & Yokoyama, T. Topological exceptional surfaces in non-Hermitian systems with parity-time and parity-particle-hole symmetries. *Phys. Rev. B* **99**, 041202 (2019).

27. Chandrasekaran, A., Shtyk, A., Betouras, J. J. & Chamon, C. Catastrophe theory classification of fermi surface topological transitions in two dimensions. *Phys. Rev. Res.* **2**, 013355 (2020).

28. Yuan, N. F. Q. & Fu, L. Classification of critical points in energy bands based on topology, scaling, and symmetry. *Phys. Rev. B* **101**, 125120 (2020).

29. Kirillov, O. N., Overton, M., Robust stability at the swallowtail singularity. *Fron. Phys.* **1**, 24 (2013).

30. Raz, O., Pedatzur, O., Bruner, B. D. & Dudovich, N. Spectral caustics in attosecond science. *Nat. Photonics*, **6**, 170-173 (2012).

31. Gajer, P., The intersection Dold-Thom theorem. *Topology* **35**, 939-967 (1996).

32. Freedman, D. Z. & Van Proeyen, A. *Supergravity* (Cambridge Univ. Press, Cambridge, 2012).

Acknowledgements: This work was supported by Research Grants Council of Hong Kong through grants AoE/P-502/20, 16307621 and 16307821, and KAUST20SC01. Y. Zhu acknowledges the financial support from National Natural Science Foundation of China (NSFC) grant 11701263. We acknowledge Prof. Zhen Lei for helpful comments in constructing the theoretical framework.

Author contributions: H.J. and C.T.C. planed the project. J.H., Y.W., H.J. and C.T.C. designed the sample. J.H. carried out the measurements. J.H. and H.J. analyzed the data. R.Y.Z., Y.Z. and H.J. constructed the theoretical framework. J.H., R.Y.Z., Y.Z., H.J. and C.T.C. wrote the manuscript. J.H., R.Y.Z., X.O., Y.Z., H.J. and C.T.C. contributed to the discussion.

Competing interests: Authors declare no competing interests.

Additional Information:

Supplementary Information is available for this paper.

Correspondence and requests for materials should be addressed to: zhuyf@sustech.edu.cn; jiahongwei7133@gmail.com; phchan@ust.hk.

Data and code availability: All data and code are available in the main text and the supplementary information.

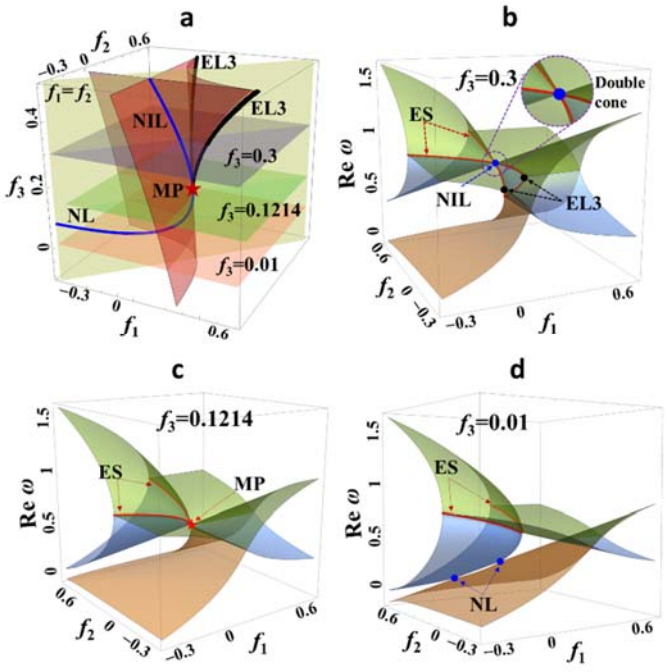

Fig. 1| Degeneracy features of eigenvalues on different cut planes in the parameter space, showing a swallowtail structure. a, Plot of swallowtail structure in 3D parameter space, obtained by solving zeros of the discriminant of characteristic polynomial of Eq. (1). Red surfaces are ESs; blue and black lines denote non-defective (NIL and NL) and defective (EL3) degeneracy lines, respectively. The meeting point (MP) is denoted by the red star. **b-d**, Eigenvalues (real part) on cut planes f_3=0.3 (blue), f_3=0.1214 (green) and f_3=0.01 (pink) of (**a**), respectively.

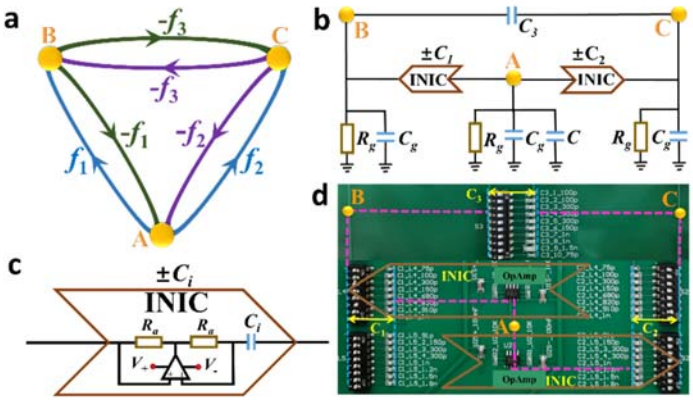

310

311 **Fig. 2| Experimental realization of the swallowtail catastrophe with a non-reciprocal**
312 **circuit system. a**, Tight-binding hoppings between each pair of nodes **A**, **B** and **C**. **b**,
313 Schematic diagram for realizing the Hamiltonian in Eq. (1). Non-reciprocal hoppings between
314 nodes **A** and **B**, and nodes **A** and **C** in the circuit system are implemented using INIC tandem
315 with capacitors (**c**); reciprocal hopping between **B** and **C** is realized with pure capacitors. **d**,
316 Photo of the main part of the PCB sample for the experiments.

317

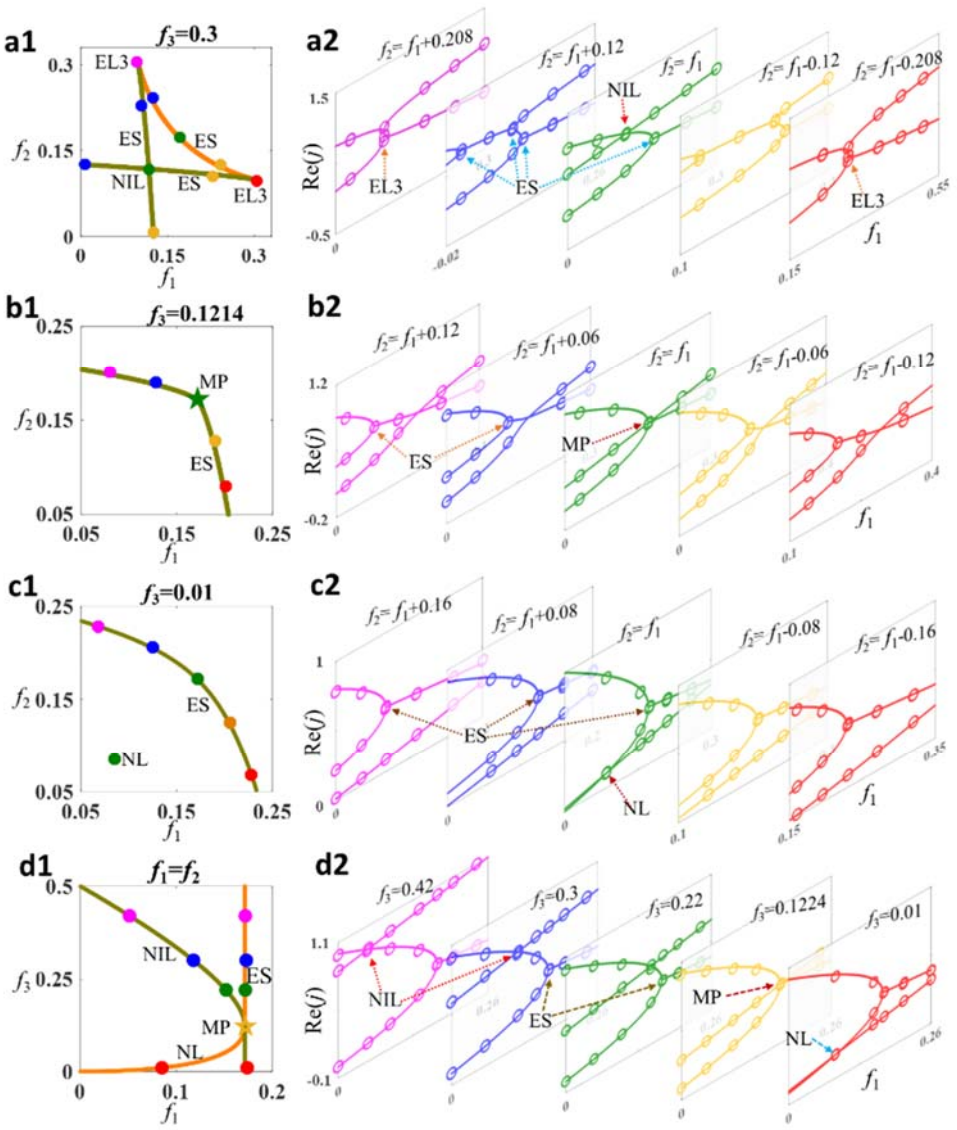

318

319 **Fig. 3| Experimental observation of swallowtail catastrophe with the circuit system. a-d**,
320 Experimental measurements of the swallowtail on planes f_3=0.3 (**a**), f_3=0.1214 (**b**), f_3=0.01 (**c**)
321 and f_1=f_2 (**d**). **a1-d1**, Degeneracies on these cut planes: orange-colored lines denote ESs and
322 NL formed by the 1nd and 2rd bands; ESs and NIL formed by the 2nd and 3rd bands are olive-
323 colored. The solid markers are degeneracies identified experimentally. **a2-d2**, Real eigenvalue
324 dispersions as a function of f_1 along different lines (f_2=f_1+s or f_3=s) on the corresponding cut
325 plane. The eigenvalues are ordered from small to large in exact phases. The measured
326 admittance eigenvalues are marked in circle.

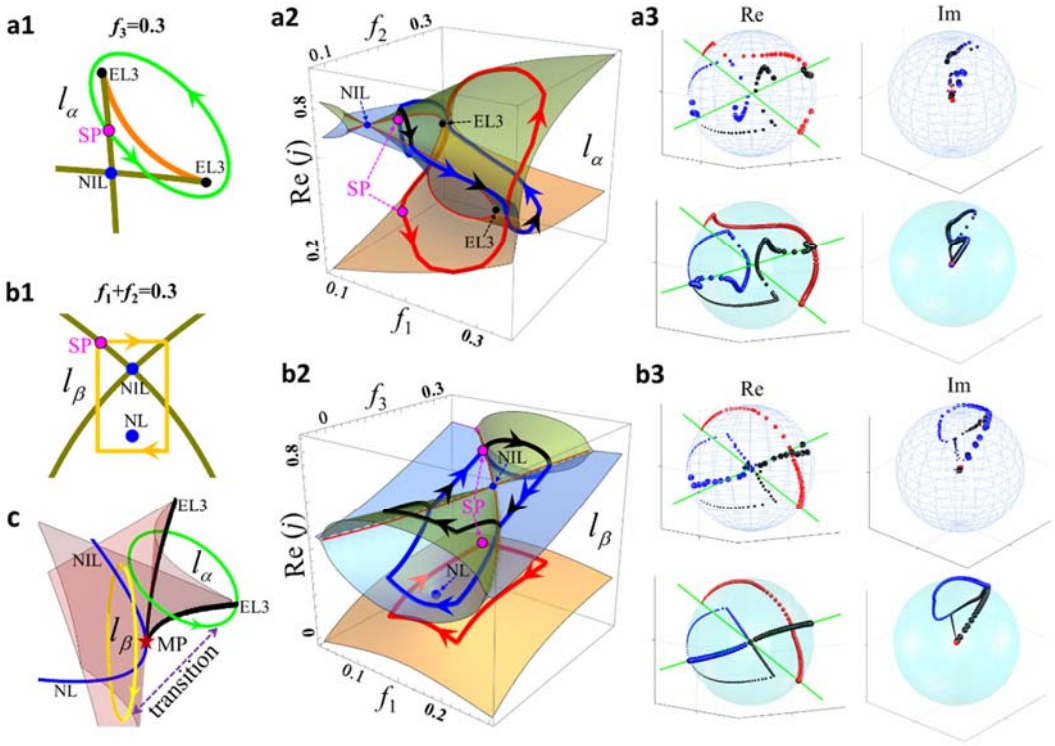

327

328 **Fig. 4| Understanding the transition of double EL3s to NIL and NL from an eigen-frame**
329 **rotation and deformation perspective. a1-b1**, Loop l_α (green) encloses the pair of EL3s, and
330 loop l_β (yellow) encloses the NIL and NL together. **a2-b2**, Trajectories of eigenvalues along
331 loops l_α and l_β, respectively. SP (purple dots) stands for the starting point. **a3-b3**, Eigen-frame
332 deformation and rotation process along loops l_α and l_β, respectively. Upper and lower panels
333 correspond to experimental and theoretical results, respectively. φ_1, φ_2 and φ_3 are colored as
334 red, blue and black, respectively. The increase of ball size denotes the variation of parameters
335 along the loops. Re and Im denote real and imaginary parts of eigenstates, respectively. **c**,
336 Illustration of the transition from double EL3s to NIL and NL in the swallowtail structure. Note
337 that in the transition process, the loop does not cut through any degeneracy lines.

338